Persistent Solar Influence on North Atlantic Climate During the Holocene

Gerard Bond, *et al.*

Science **294**, 2130 (2001);
DOI: 10.1126/science.1065680

47. L. Seress, H. Abraham, T. Tornoczky, Gy. Kosztolanyi, *Neuroscience* **105**, 831 (2001).
48. P. Rakic, *Nature Neurosci.* **1**, 643 (1998).
49. B. Kirschenbaum *et al.*, *Cereb. Cortex* **4**, 576 (1994).
50. F. Doetsch, I. Caille, D. A. Lim, J. M. Garcia-Verdugo, A. Alvarez-Buylla, *Cell* **97**, 703 (1999).
51. F. H. Gage, *Science* **287**, 1433 (2000).
52. E. D. Laywell, P. Rakic, V. G. Kukekov, E. C. Holland, D. A. Steindler, *Proc. Natl. Acad. Sci. U.S.A.* **97**, 13883 (2000).
53. A. Bjorklund, O. Lindvall, *Nature Neurosci.* **3**, 537 (2000).
54. R. McKay, *Nature* **406**, 361 (2000).
55. A. Privat, *Int. Rev. Cytol.* **40**, 281 (1975).
56. D. R. Kornack, P. Rakic, data not shown.
57. We thank P. S. Goldman-Rakic, E. A. Markakis, and N. Sestan for insightful comments. Supported by grants NS14841 and EY02593 from the United States Public Health Service.

17 August 2001; accepted 24 October 2001

Persistent Solar Influence on North Atlantic Climate During the Holocene

Gerard Bond,[1]* Bernd Kromer,[2] Juerg Beer,[3] Raimund Muscheler,[3] Michael N. Evans,[4] William Showers,[5] Sharon Hoffmann,[1] Rusty Lotti-Bond,[1] Irka Hajdas,[6] Georges Bonani[6]

Surface winds and surface ocean hydrography in the subpolar North Atlantic appear to have been influenced by variations in solar output through the entire Holocene. The evidence comes from a close correlation between inferred changes in production rates of the cosmogenic nuclides carbon-14 and beryllium-10 and centennial to millennial time scale changes in proxies of drift ice measured in deep-sea sediment cores. A solar forcing mechanism therefore may underlie at least the Holocene segment of the North Atlantic's "1500-year" cycle. The surface hydrographic changes may have affected production of North Atlantic Deep Water, potentially providing an additional mechanism for amplifying the solar signals and transmitting them globally.

A prominent feature of the North Atlantic's Holocene climate is a series of shifts in ocean surface hydrography during which drift ice and cooler surface waters in the Nordic and Labrador Seas were repeatedly advected southward and eastward, each time penetrating deep into the warmer strands of the subpolar circulation (*1*, *2*). The persistence of those rather dramatic events within a stable interglacial has been difficult to explain. Earlier work (*3*) suggested that a low-resolution record of North Atlantic drift ice in the early Holocene may have been linked to the energy output of the Sun. The likelihood of any such strong climate response to solar variability has long been debated because the magnitude of the forcing is small. Results of recent atmospheric general circulation (GCM) mod-

[1]Lamont-Doherty Earth Observatory of Columbia University, Route 9W, Palisades, NY 10964, USA. [2]Heidelberg Academy of Sciences, Institute of Environmental Physics, INF 229, D-69120 Heidelberg, Germany. [3]Eidgenössische Anstalt für Wasserversorgung, Abwasserreinigung und Gewuässerschutz, Ueberlandstrasse 133, Postfach 611, CH-8600 Duebendorf, Switzerland. [4]Laboratory of Tree-Ring Research, University of Arizona, 105 West Stadium, Tucson, AZ 8572, USA. [5]Department of Marine, Earth and Atmospheric Sciences, North Carolina State University, 1125 Jordan Hall, Raleigh, NC 27695–8208, USA. [6]Accelerator Mass Spectrometry ^{14}C Lab, ITP Eidgenössische Technische Hochschule Hoenggerberg, CH-8093 Zurich, Switzerland.

*To whom correspondence should be addressed. E-mail: gcb@ldeo.columbia.edu

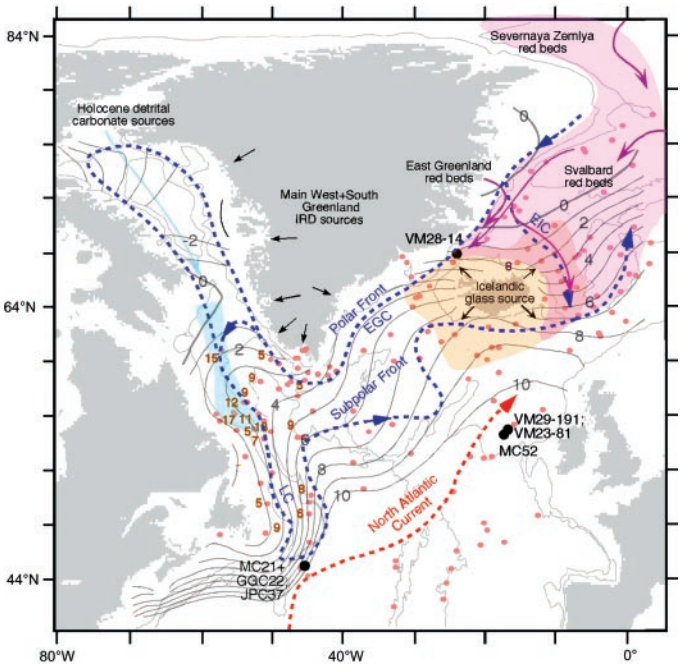

Fig. 1. Map of coring sites described in the text that provide the basis for inferring sources and transport routes of ice carrying the petrologic tracers. Dashed blue lines: subpolar cyclonic circulation. The main frontal boundaries are labeled in blue. Red dots are core-top measurements of all tracers. Areas enclosed by shading indicate core tops with >10% of tracers as keyed by colors [red: >10% hematite-stained grains (HSG); yellow: >10% Icelandic glass (IG); blue: >10% detrital carbonate (DC)]. Documentation for core-top percentages of HSG and IG are from (*2*); red numbers next to core-top locations are percentages of DC in core tops. Colored arrows indicate inferred direction of transport of tracer-bearing drift ice. Gray lines are mean (1900 to 1992) ocean-surface temperatures from LEVITUS94 (*52*) for spring when iceberg discharge into the North Atlantic reaches a maximum. EIC: East Iceland Current; EGC: East Greenland Current; LC: Labrador Current. VM28-14: 64°47′N, 29°34′W, 1855-m water depth; VM29-191: 54°16′N, 16°47′W, 2370-m water depth; VM23-81: 54°15′N, 16°50′W, 2393-m water depth; KN158-4 MC52: 55°28′N, 14°43′W, 2172-m water depth; KN158-4 MC21, KN158-4 GGC22: 44°18′N, 46°16′W, 3958-m water depth; and EW9303 JPC37: 43°58′N, 46°25′W, 3980-m water depth. Petrologic analyses of more than 120 core tops demonstrates that most tracer-bearing ice today circulates in the cooler waters north and west of the subpolar front. Lower tracer percentages to the south and east are consistent with observational evidence that icebergs there come mainly from south and west Greenland where tracer-bearing rock types are rare, if present at all. Increases in DC off Newfoundland, therefore, reflect southward shifts of the cooler Labrador Sea surface water and carbonate-bearing drift ice. Peak percentages of HSG and IG off Newfoundland rarely reach the corresponding peak values of those two tracers in the eastern North Atlantic (MC52-VM29-191) (Fig. *2*). That rules out transport of HSG and IG through the East Greenland–Labrador Sea current system at times of peak drift-ice transport. The eastern North Atlantic drift-ice records, therefore, require that at times of peak tracer percentages, ice-bearing surface waters from north of Iceland were advected southeastward toward the coring site. That was accompanied by cooler ocean-surface temperatures (*1*) and, by analogy with transport mechanisms of modern drift ice (*53*), must have been aided by northerly or northeasterly surface winds in the Nordic Seas and eastern subpolar North Atlantic. The concentrations of IRD (lithic grains >150 μm), although small, covary with the petrologic tracers, and peak percentages reflect true increases in the tracer concentrations rather than dilution by other grain types.

eling, however, have shown that a decrease of only ~0.1% in solar activity over the 11-year sunspot cycle could produce a change in surface climate through the atmosphere's dynamic response to changes in stratospheric ozone and temperature (*4*, *5*). Here we test the solar-climate connection by comparing high-resolution measurements of drift ice in three North Atlantic deep-sea cores with proxies of changes in solar irradiance through the entire length of the Holocene.

The marine and nuclide records. Our proxies for changes in Holocene drift ice are the percentages of three petrologic tracers in the small amounts of ice-rafted debris that are ubiquitous in the subpolar North Atlantic: hematite-stained grains (HSG), Icelandic glass (IG), and detrital carbonate (DC). As demonstrated previously, the tracers are particularly sensitive to changes in the amounts and trajectories of glacial ice and/or sea ice circulating in the surface waters (*1*, *2*). We interpret percentage increases in the tracers as reflecting advections of cooler, ice-bearing surface waters eastward from the Labrador Sea and southward from the Nordic Seas, probably accompanied by shifts to strong northerly winds north of Iceland, as explained in Fig. 1 and (*1*).

Chronologies of the drift-ice records from the three coring sites [Fig. 1 and supplementary note (*1*); supplementary Web material is available on *Science* Online at www.

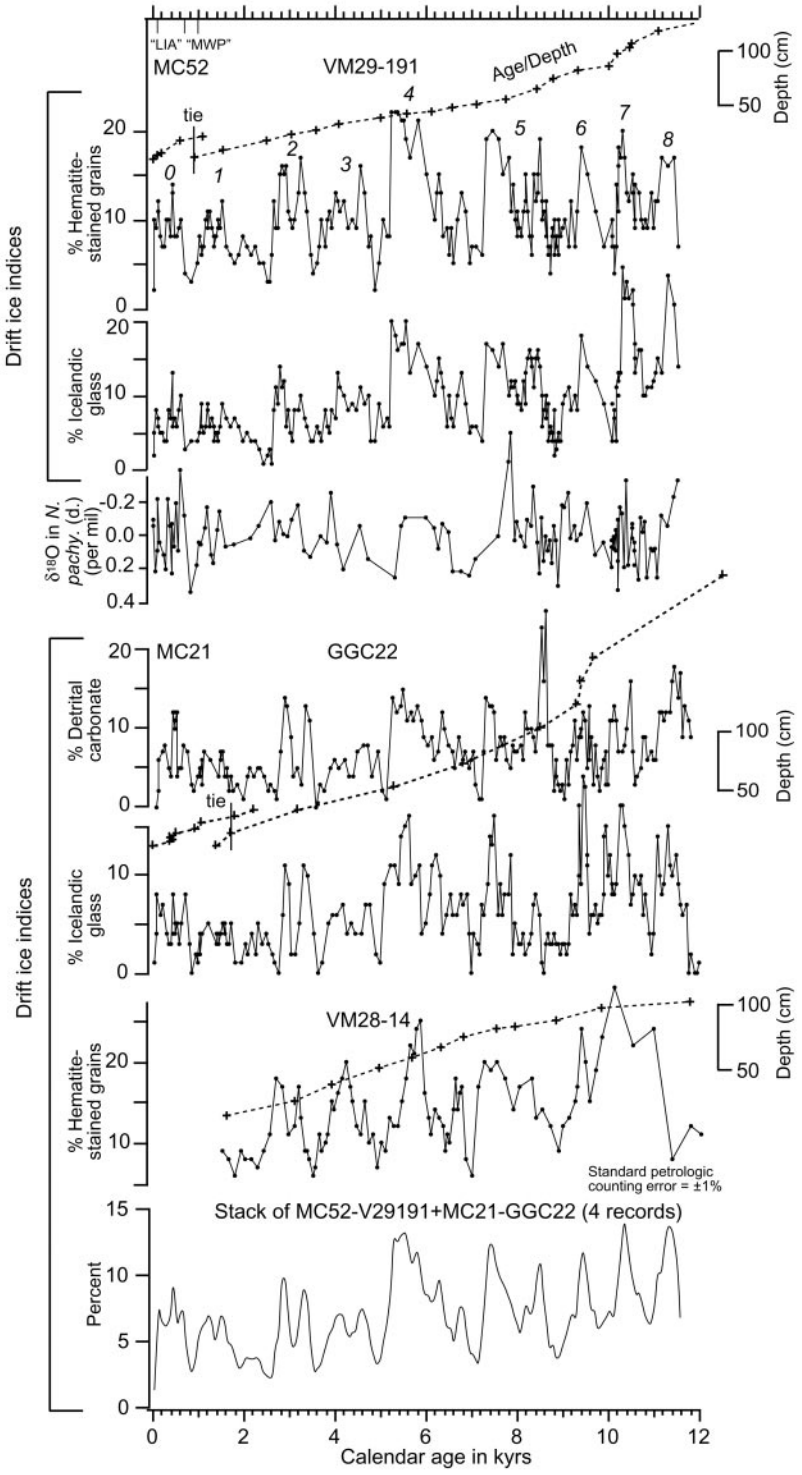

Fig. 2. Holocene records of drift ice (as percentage variations in petrologic tracers; see text) and planktic $\delta^{18}O$ from *Neogloboquadrina pachyderma* (d.) for MC52-VM29-191. The petrologic tracers of drift ice are detrital carbonate, fresh volcanic glass from Iceland, and hematite-stained grains, expressed as percentages of lithic grains (ice-rafted debris) in the 63- to 150-μm size range. The standard error in the petrologic measurements is ±1% (*1*). All core locations are shown in Fig. 1. "Tie" denotes points at which multicore (MC) records were patched into gravity and piston core records from the same sites to extend time series to the present (all MC core tops contain bomb radiocarbon, i.e., negative corrected radiocarbon ages; all reservoir corrections are −400 years). Age depth models are from Web table 1. The stacked record was calculated by averaging all detrended and resampled records except from VM28-14. The rationale for stacking is that all five records are in % petrology and each petrologic tracer reflects the same parameter, i.e., change in drift ice. Numbers 0 to 8 designate the millennial-scale cycles recognized in earlier work and regarded as part of the North Atlantic's "1500-year" cycle (*1*). The new records here demonstrate that the numbered millennial-scale variations reflect a modulation of the baseline of the centennial-scale cycles. Planktic $\delta^{18}O$ of *N. pachyderma* (d.) was measured on hand-picked specimens >150 μm and analyzed by W. Showers as outlined in (*1*). The isotopic record was detrended linearly to remove a long-term trend that reflects an apparent combination of ice-volume decrease and Neoglacial cooling.

sciencemag.org/cgi/content/full/1065680/DC1] are constrained by 59 calibrated accelerator mass spectrometer radiocarbon dates (Fig. 2 and Web table 1; all ages are in calendar ages before the present unless otherwise indicated). Our best-resolved record, MC52-VM29-191, was dated on average every 500 years. Bioturbation of the sediment is so low that core tops have modern radiocarbon (negative corrected ^{14}C ages) even where sedimentation rates are 10 to 15 cm/10^3 years; we increased sampling resolution to 20 years in places and still resolved abrupt shifts in the tracers across intervals as short as 70 years (Fig. 2). Sample resolution in most of the records is between 30 and 50 years.

The production rates of cosmogenic nuclides are related to the solar winds and solar activity. Higher production rates are associated with weaker winds and reduced irradiance (*6*). We used two proxies that for the Holocene are regarded as evidence of production rates or a combination of production rates and ocean forcing: a record of ^{10}Be measurements from Greenland ice cores converted to a ^{10}Be flux (*7*, *8*), and a record of ^{14}C from the $\Delta^{14}C$ in tree rings (*9*) corrected for marine and terrestrial reservoir effects (*10*).

Linking records of drift ice and nuclide production rate. Our drift-ice records contain a series of rapid, centennial-scale cycles (mostly 200 to 500 years) closely matching large shifts in the nuclide production rates (Fig. 3) (the term "cycle" here does not imply periodicity). In the early Holocene three prominent, mainly single-peaked, centennial-scale cycles have nearly the same ages in all of the records. Between 0 and 9000 years ago centennial-scale cycles are grouped into distinct, nonrepeating composite cycles that

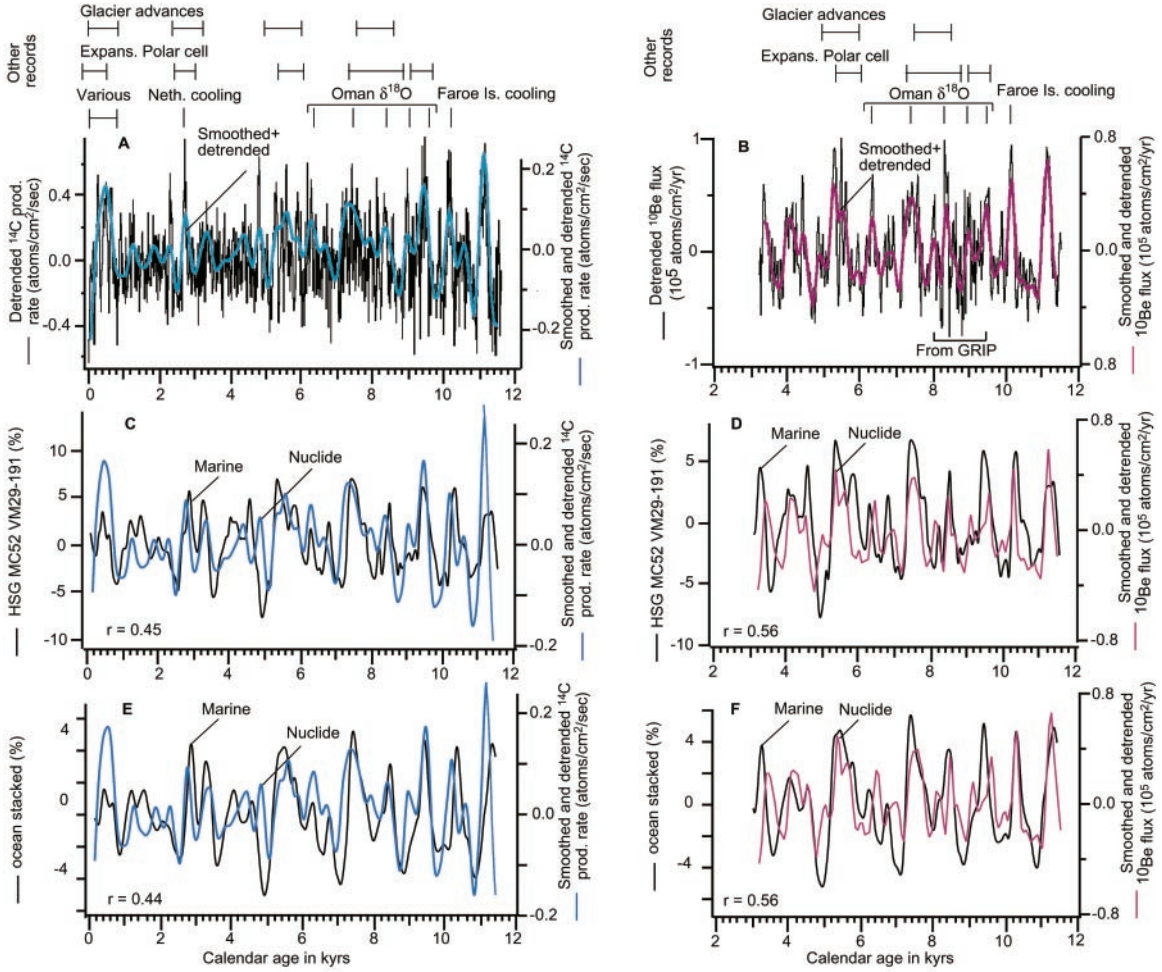

Fig. 3. Comparison of ^{10}Be and ^{14}C records with time series of MC52-VM29-191 and stacked marine records. ^{14}C production rate (see text) of 0.8 atoms cm^{-2} s^{-1} = atmospheric $\Delta^{14}C$ of 25‰. A complete detailed ^{10}Be record for the Holocene has not been measured in the GRIP or GISP2 ice cores. From 3300 to 11,500 years ago we use a composite of ^{10}Be from both cores (*7*, *8*) placed on the GISP2 time scale (Fig. 3B). We use the GISP2 time scale because most of ^{10}Be was measured in that core. Comparison of the records on the different time scales indicates an age difference of about 50 years. Transfer of the GRIP data to the GISP2 time scale was constrained by the 8200-year $\delta^{18}O$ peak and by the abrupt shift in $\delta^{18}O$ at the end of the Younger Dryas present in both records. Error in the age transfer is probably smaller than 50 years. We converted the ^{10}Be concentrations measured in Greenland ice to fluxes, although over the last 10,000 years snow accumulation at Summit was constant enough that flux and concentration are essentially interchangeable (*54*, *55*). From 10,000 to 11,500 years, accumulation rates increased linearly by about 30% (*54*, *55*), and any error in flux estimates in that interval is small on the short time scales of interest here. ^{10}Be measurements from the present to 3300 years ago are not yet available from Summit cores, and published Camp Century and Dye 3 ^{10}Be for that interval (*56*) has insufficient resolution for our purposes. To remove long-term components of the nuclide and marine records that are not of interest, we first filtered the raw time series with a gaussian band-pass filter designed to remove all energy at periods >1800 years and then subtracted the filtered results from the unfiltered records. (The long-term trends in the records leaked through a band-pass filter of the millennial-centennial compo-nents.) The detrended nuclide records were smoothed by using a binomial function with a smoothing window of 70 years (which is the mean resolution of the marine records). Marine and nuclide records were then resampled at equally spaced 70-year intervals. Detrended nuclide records are shown in black in (A) and (B); smoothed nuclide records are in color. The prominent bundles of centennial cycles correspond in part to the "triple events" recognized in the residual $\Delta^{14}C$ and correlated to the ionic time series from the GISP2 ice core (*16*, *18*). Bars and vertical lines above (A) and (B) mark possible correlatives of the paired drift ice–nuclide peaks with previous efforts to match paleoclimate records with changes in solar irradiance. Glacier advances are from Scandinavian records (*15*); expansion of Polar cell is from ionic time series in GISP2 ice core (*16*); Netherlands cooling event is from (*17*); Faroe Island cooling event is from (*18*); and Oman $\delta^{18}O$ record, as proxy of rainfall, is from (*19*). "Various" refers to records from the Sargasso Sea (*20*), offshore of West Africa (*21*), the Cariaco Basin (*22*), equatorial lakes in East Africa (*23*), and the Yucatan Peninsula (*24*).

tightly constrain the correlation (Figs. 2 and 3). The same cyclic patterns are present in a single, well-resolved record from the eastern North Atlantic, MC52-VM29-191, and in a stack of four drift-ice records from the eastern and western sites, demonstrating that the patterns are the dominant features of the regional drift-ice variability (Fig. 2). The correlation coefficients between the nuclide production records and both the individual and the stacked marine records range from r = 0.44 to 0.56 (Fig. 3). The correlation coefficient between the two detrended and smoothed nuclide records is r = 0.6. The visual match among the records can be improved by adjusting the marine time series within chronological error (Web fig. 1). Coherency between the solar and marine proxies was estimated with two methods, cross-spectral analysis (*11*) and singular spectrum analysis (*12*), which demonstrated statistically significant coherency among the records in both the centennial and millennial bands [see (*13*) and Web fig. 2 for details].

The smoothed nuclide peaks we have matched with drift-ice peaks correspond to intervals in the unsmoothed nuclide records with a few to several rapid (100- to 200-year), conspicuously large-amplitude variations in production rates. The interval from 5000 to 6000 years ago is a good example (Fig. 3). It is highly unlikely that Holocene climate forcing alone could have produced such large and abrupt production-rate changes at essentially the same time in both nuclides [see discussion in note (*14*)]. Our correlations are evidence, therefore, that over the last 12,000 years virtually every centennial time scale increase in drift ice documented in our North Atlantic records was tied to a distinct interval of variable and, overall, reduced solar output.

A solar influence on climate of the magnitude and consistency implied by our evidence could not have been confined to the North Atlantic. Indeed, previous studies have tied increases in the $\Delta^{14}C$ of tree rings, and hence, reduced solar irradiance, to Holocene glacial advances in Scandinavia (*15*); expansions of the Holocene Polar atmospheric circulation above Greenland (*16*); an abrupt cooling in the Netherlands about 2700 years ago (*17*); and lacustrine records from the Faroe Islands (*18*). All of these events closely match prominent increases in North Atlantic drift ice (Fig. 3, A and B). Well-dated, high-resolution measurements of $\delta^{18}O$ in a stalagmite from Oman document five episodes of reduced rainfall at times of strong solar minima centered on 6300, 7400, 8300, 9000, and 9500 years ago (*19*). Each of those episodes also corresponds to paired intervals of reduced solar irradiance and increases in North Atlantic ice drift in our records (Fig. 3, A and B). The most recent drift-ice cycle, between about 100 and 1100 years ago, corresponds to temperature cycles in the Sargasso Sea (*20*) and in the upwelling region off West Africa (*21*), suggesting a broad regional response in the subpolar and subtropical North Atlantic. The interval also encompasses a series of marked increases in surface ocean upwelling in the Cariaco Basin, prominent changes in lake levels in equatorial east Africa, and distinct episodes of drought in the Yucatan Peninsula, all of which have been linked to episodes of reduced solar irradiance (Fig. 3) (*22–24*).

The last drift-ice cycle is broadly correlative with the so-called Little Ice Age (LIA) and Medieval Warm Period (MWP) (Fig. 2). Although the regional extent and exact age of those two events are still under debate, our records support previous suggestions that both may have been partly or entirely linked to changes in solar irradiance (*25*). The large 2σ errors in calibrated ages (typically between $\pm$100 and $\pm$150 years) (Web table 1), however, preclude any direct comparison of our drift-ice indices or the subtropical North Atlantic temperature records with the distinct decades-long Wolfe, Spörer, Maunder, and Dalton solar minima (*26*). However, the solar-climate links implied by our record are so dominant over the last 12,000 years that it seems almost certain that the well-documented connection between the Maunder solar minimum and cold decades of the LIA could not have been a coincidence.

The comparisons we have outlined imply that the footprint of the solar impact on climate extended from polar to tropical latitudes. Moreover, as suggested especially by our comparison with the Oman record, the broad teleconnective response to strong solar minima appears to link cooler ice-bearing surface waters in high northern North Atlantic latitudes with episodes of reduced monsoon activity and reduced rainfall in at least parts of the low latitudes.

The distinct, longer cycles of millennial duration, as defined by the grouping of the centennial oscillations, correspond to the nine cycles of the Holocene identified in lower-resolution records of earlier work and indicated by the numbered events in Fig. 2. Those drift-ice cycles compose part of an enigmatic, at best quasi-periodic, "1500-year" cycle that appeared to persist across the glacial termination and well into the last glaciation, suggesting that the cycle is a pervasive feature of the climate system (*1*, *2*, *27*). Thus, as anticipated more than 20 years ago by Denton and Karlén (*15*), at least the Holocene segment of the North Atlantic's "1500-year" cycle appears to have been linked to variations in solar irradiance. If that is correct, it is unnecessary to invoke either internally forced oscillations in the deep ocean's circulation (*28*) or longer-term internally and orbitally forced modulations of atmospheric variability,

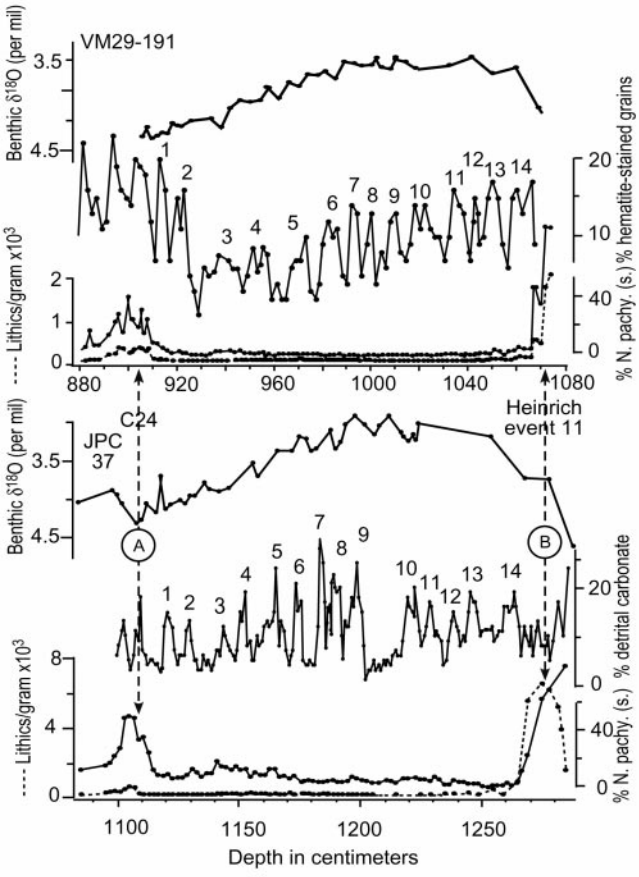

Fig. 4. Records of MIS 5e (Marine Isotope Stage 5e) from VM29-191 and JPC 37 (located in Fig. 1). Benthic $\delta^{18}O$ from *Cibicidoides. wuellerstorfi* [(*57*) and augmented in this study]. Lithic and *N. pachyderma* (s.) are from (*57*, *58*). Percent DC and HSG were measured in the same way as for Holocene records. Tie point A is a widespread, brief cooling event (C24) corresponding to MIS 5d, and tie point B is an abrupt Heinrich event, 11, both inferred to be synchronous throughout the subpolar North Atlantic (*58–60*).

such as El Niño–Southern Oscillation and the North Atlantic Oscillation (*29*), as primary forcing mechanisms of centennial to millennial time-scale changes in the North Atlantic's Holocene climate. This does not preclude the possibility that solar forcing may excite those modes of atmospheric variability.

At two of our coring sites, we have identified a series of variations within all of the previous interglacial, MIS (Marine Isotope Stage) 5e records that are markedly similar to those of the Holocene. Measurements of two of the drift-ice indices reveal the same number of events between chronological markers (Figs. 1 and 4), suggesting that, as for their Holocene counterparts, they are correlative across the subpolar North Atlantic. Assuming that 20,800 years separates the markers as indicated by SPECMAP chronology (*30*), the mean duration of the stage 5e cycles is 1480 years, comparable to the 1340-year mean duration of the Holocene cycles. To the extent these findings document a common origin for the Holocene and MIS5e drift-ice records, they raise the strong possibility that solar forcing also influenced centennial- and millennial-scale variability of past interglacial climates.

If solar forcing remains as the most likely cause of the Holocene centennial- and millennial time-scale variations in the North Atlantic's drift-ice record, it adds an additional and unexplored dimension to the problem of how solar variability could induce a climate change. GCM modeling of the amplifying mechanisms have focused on the atmosphere's dynamic response to solar forcing (*4*, *5*). The models imply that at times of reduced solar irradiance, the downward-propagating effects triggered by changes in stratospheric ozone lead to cooling of the high northern latitude atmosphere, a slight southward shift of the northern subtropical jet, and a decrease in the Northern Hadley circulation. Those atmospheric responses to reduced irradiance could perhaps lead to the coincident increases in North Atlantic drift ice, cooling of both the ocean surface and atmosphere above Greenland, and the reduced precipitation in low latitudes implied by our findings in Fig. 3.

Potential feedback from changes in thermohaline circulation. Results of recent modeling suggest that the North Atlantic's climate response to an estimated ~0.25% irradiance decrease over the short Maunder Minimum (~70 years) would resemble a reduced AO/NAO (*31*). Comparison of the last three drift-ice cycles with temperature variations in Europe, Greenland, and the subtropical North Atlantic, however, indicates that on the much longer multicentennial to millennial time scales of our records, the regional coolings are discordant with the distinct AO/NAO dipole anomaly patterns (Fig. 5, A and B). Adjusting the marine chronologies within the 2σ ranges of the radio-

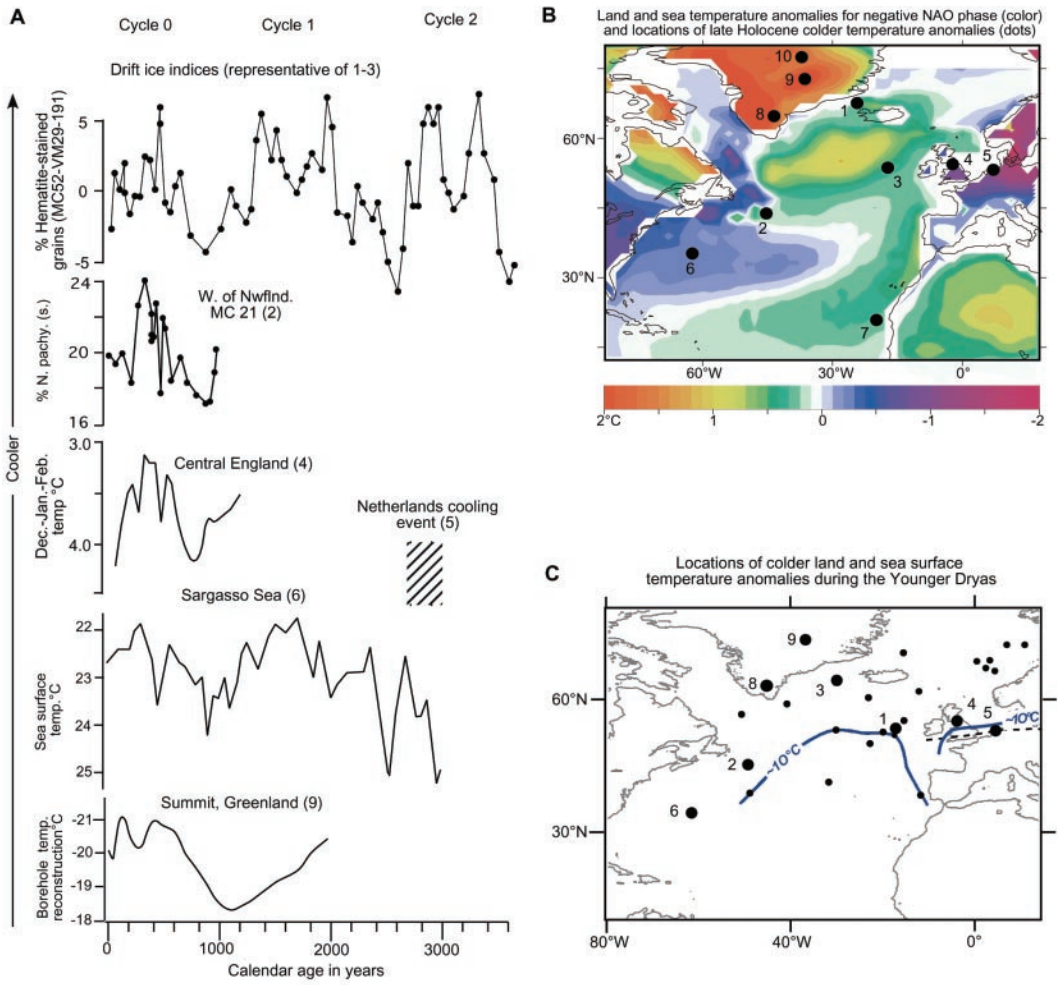

Fig. 5. (**A**) Comparison of drift-ice indices from Fig. 2 for cycles "0-2" with the *N. pachyderma* (sinistral) record from MC21, the observational temperature record from central England (*61*), cooling event from the Netherlands (*17*), the Sargasso Sea temperature record (*19*), and air temperature from Summit, Greenland, borehole temperature reconstructions (*62*). Calibrated ages and errors are from Web table 1. Locations are shown in (B). (**B**) Representative temperature-anomaly pattern during a reduced AO/NAO and locations (solid dots) of regional cooling events in (A) together with upwelling site at 7 (*20*), Dye 3 ice core at 8 (*62*), and north Greenland ice cores at 10 (*63*). Land temperature anomalies were calculated by regressing the NAO index (*64*) to the winter-averaged National Centers for Environmental Prediction–National Center for Atmospheric Research reanalysis data (1958 to 1999, December to April), whereas the ocean sea-surface temperature anomalies were computed by an ocean model's response to NAO wind anomalies regressed to the winter-averaged NCEP-NCAR reanalysis with a 12-year fixed period (*65*, *66*). On the multicentennial to millennial time scales of our records, the regional cooling patterns in (A) are discordant with the AO/NAO temperature anomaly dipoles. (**C**) Dots are locations where sea-surface temperature estimates during the Younger Dryas were cooler relative to what immediately preceded and followed that interval. Numbered, large dots are as documented in (B); small dots are from (*67*–*72*); the blue isotherm is for Younger Dryas temperature estimates in (*67*–*72*). The broad regional cooling pattern is thought to result from a reduction in NADW formation as documented for the Younger Dryas (*1*)—a pattern that also contrasts with the typical dipole temperature anomalies of a reduced AO/NAO as in (B). However, a similar comparison on the decadal time scale of the Maunder Minimum (~70 years) is impossible, owing to the large calibrated ^{14}C errors. A recent estimate of sea-surface warming at a single site in the Laurentian fan off the Scotian margin during the LIA (*73*) is not replicated a short distance away at our site MC21 (Figs. 1 and 5A).

carbon calibrations (Web table 1) cannot force the pattern of temperature changes into agreement with those of the AO/NAO. That conclusion is best demonstrated for the last millennium and is implied for the previous two cycles (1 and 2) where data are available (Fig. 5A).

The regional cooling patterns of the last three cycles instead resemble those that result from reduced NADW (North Atlantic Deep Water) formation, as exemplified by the distribution of the much larger temperature decreases accompanying the episode of reduced NADW formation during the Younger Dryas (Fig. 5C) (*1*). Measurements of deep-circulation proxies, although somewhat equivocal, suggest reduced NADW production during at least some of the drift-ice peaks (*1*, *32*). In addition, because decreases in planktic $\delta^{18}O$ in MC52-VM29-191 correspond to drift-ice increases (Fig. 2) and cooler surface temperatures (*1*), surface salinities must have decreased, perhaps by as much as 0.5 to 0.6 salinity units (*33*). Such relatively large surface salinity decreases within the convecting regions of the North Atlantic could well have caused reductions in NADW formation (*34*).

An additional amplifying mechanism, therefore, may have been solar-triggered reductions in North Atlantic thermohaline overturning, especially if accompanied by increased sea-ice fluxes into the Nordic Seas (*34*, *35*). Indeed, during the late 1960s to late 1970s an increase in windblown Artic drift ice through the Fram Strait resulted in a surface water freshening of up to 0.4 to 0.6 salinity units in the Nordic Seas and subpolar North Atlantic [the Great Salinity Anomaly (34)], falling within the range of the salinity decreases implied by our planktic $\delta^{18}O$ measurements at the easternmost site (Fig. 2). The freshening reduced convection in the Labrador Sea (*34*, *36*) and, in contrast to the temperature anomaly dipoles of a reduced AO/NAO, surface ocean cooling was basin wide (*37*). The high-pressure anomaly over Greenland intensified, producing abnormally strong northerly winds that spread Nordic Sea drift ice southward into the subpolar North Atlantic, not unlike our inference of southerly drift-ice transport over the two northernmost coring sites during the peak drift-ice episodes of the Holocene (Fig. 1). It is intriguing that this possible modern analog of the more dramatic conditions we infer for the Holocene falls within the largest reversal in the overall rise of solar irradiance during the 20th century (Web fig. 3) (*38*).

The Arctic-Nordic Seas thus may have been a key region where solar-induced atmospheric changes were amplified and transmitted globally through their impact on sea ice and North Atlantic thermohaline overturning. Reduced northward heat transport, moreover, could have further altered North Atlantic latitudinal temperature and hydrologic gradients, potentially enhancing the climate response in low-latitude climates [e.g., (*39*)].

The results of this study demonstrate that Earth's climate system is highly sensitive to extremely weak perturbations in the Sun's energy output, not just on the decadal scales that have been investigated previously, but also on the centennial to millennial time scales documented here. The apparent solar response was robust in the North Atlantic even as early Holocene vestiges of the ice sheets continued to exert a climate influence and as the orbital configuration shifted from that of the Holocene optimum to the quite different regime of the last few thousand years. Our findings support the presumption that solar variability will continue to influence climate in the future, which up to now has been based on extrapolation of evidence from only the last 1000 years (*25*). If forcing of North Atlantic ice drift and surface hydrography is fundamentally linked to the Sun and begins in the stratosphere, then atmospheric dynamics and their link to the ocean's circulation are much more important for interpreting centennial and millennial time scales of climate variability than has been assumed.

References and Notes

1. G. C. Bond *et al*., *Science* **278**, 1257 (1997).
2. G. C. Bond *et al*., in *Mechanisms of Global Climate Change at Millennial Time Scales*, P. Clark, R. Webb, L. D. Keigwin, Eds. (Geophysical Monograph Series 112, American Geophysical Union, Washington, DC, 1999), pp. 35–58.
3. M. Friedrich, B. Kromer, M. Spurk, J. Hofmann, K. Kaiser, *Quat. Int.* **61** (1999).
4. J. Haigh, *Science* **272**, 981 (1996).
5. D. Shindell, D. Rind, N. Balachandran, J. Lean, P. Lonergan, *Science* **284**, 305 (1999).
6. J. Masarik, J. Beer, *J. Geophys. Res.* **104**, D10, 12099 (1999).
7. R. C. Finkel, K. Nishiizumi, *J. Geophys. Res.* **102**, C12, 26699 (1997).
8. F. Yiou *et al*., *J. Geophys. Res.* **102**, C12, 26783 (1997).
9. M. Stuiver *et al*., *Radiocarbon* **40**, 3, 1041 (1998).
10. P. Reimer calculated a ^{14}C production rate for us from the INTCAL98 $\Delta^{14}C$ tree-ring data set using a four-box carbon-cycling model (atmosphere, oceanic mixed layer, deep sea, and the biosphere) from (*40*).
11. D. Paillard, L. Labeyrie, P. Yiou, *Eos Trans. AGU* **77**, 379 (1996).
12. R. Vautard, M. Ghil, *Physica* **D58**, 95 (1992).
13. A Blackman-Tuckey cross-spectral analysis (*11*) was applied to the smoothed and detrended records of ^{14}C and ^{10}Be production rates and to the detrended HSG in MC52-VM29-191 (shown graphically in Web fig. 2). For HSG and ^{10}Be, 70-year sampling interval, 95% confidence interval, 48 lags, and 0.000557 cycles/year bandwidth were used. Coherency in a 300- to 500-year band is 0.75 and in a 900- to 1100-year band is 0.93. For HSG and ^{14}C, 70-year sampling interval, 95% confidence interval, 69 lags, and 0.00039 bandwidth were used. Coherency in both the 300- to 500-year and 900- to 1100-year band is 0.84. We also used singular spectrum analyses (*14*) to decompose the same records into millennial (1000 to 2000 years) and centennial (300 to 500 years) components and found statistically significant coherence between the millennial components of the records. Singular spectrum analyses (SSA) were performed with an embedding dimension of 30, or 20 to 25% of the time-series lengths. Only the leading four to six empirical orthogonal functions, which cumulatively described 75 to 80% of the variance in the detrended and smoothed records, were retained in these analyses. Standard Fourier analyses were used to aggregate individual reconstructed component time series into the millennial- and submillennial-frequency time series. Quasi-coherences were then computed between these SSA time series corresponding to the solar and marine proxies. For the marine and ^{14}C records the coherency is 0.53 and is significant at >90% with nine effective degrees of freedom; for marine and ^{10}Be records the coherency is 0.74 and is significant at >95% with seven effective degrees of freedom; and for ^{10}Be and ^{14}C records the coherency is 0.76 and is significant at >95% with seven effective degrees of freedom. Coherence between submillennial components of the HSG and ^{14}C records of 0.23 with 17 effective degrees of freedom is not significant at the >90% level.
14. A box diffusion carbon cycle model (*41*) implies that a $\Delta^{14}C$ increase of 25‰ in 100 years (equivalent to a production-rate increase of about 0.8 atoms cm^{-2} s^{-1} during the large century-scale events shown in Fig. 3B) would require a 50% reduction in global ocean mixing. Coupled climate–carbon cycle models suggest that even for large, millennial-scale climatic variations such as during the Younger Dryas, $\Delta^{14}C$ would change only 10 to 40% (*42*); similarly, carbon reservoir models suggest that a 30% change in production rate over ~200 years would require a two-thirds reduction in global wind speeds relative to the current average (*43*). There is no evidence of such large ocean/climate forcing in the North Atlantic during the Holocene (*1*); the "8200-year" cold event, regarded by some as the most extreme climatic event of the Holocene (*44*), does not stand out conspicuously in either the $\Delta^{14}C$ or ^{10}Be records relative to Holocene baselines (Fig. 3, A and B), nor does the event at about 10,300 years ago, which appears to be associated with a modest decrease in NADW production (*1*). It has been further demonstrated from box models that over the entire Holocene, centennial-scale $\Delta^{14}C$ changes calculated from a ^{10}Be-based ^{14}C production rate agree well in both amplitude and phasing (generally within several percent) with the measured $\Delta^{14}C$ variations (*45*–*47*). Because ^{10}Be and ^{14}C have significantly different geochemical behavior, it is highly unlikely that climate forcing alone could have produced such similar changes in the two nuclides. Over the last 7000 years centennial-scale variations in ice core ^{10}Be flux appear to correlate well between Greenland and Antarctica (*48*), also consistent with production as the dominant control.
15. G. H. Denton, W. Karlen, *Quat. Res.* **3**, 155 (1973).
16. S. R. O'Brien *et al.*, *Science* **270**, 1962 (1995).
17. B. van Geel, J. Buurman, H. T. Waterbolk, *J. Quat. Sci.* **11**, 6, 451 (1996).
18. S. Björck *et al*., *Geology*, in press.
19. U. Neff *et al*., *Nature* **411**, 290 (2001).
20. L. Keigwin, *Science* **274**, 1504 (1996).
21. P. deMenocal, J. Ortiz, T. Guilderson, M. Sarnthein, *Science*, **288**, 2198 (2000).
22. D. E. Black *et al*., *Science* **286**, 1709 (1999).
23. D. Verschuren, K. R. Laird, B. F. Cumming, *Nature* **403**, 410 (2000).
24. D. A. Hodell, M. Brenner, J. H. Curtis, T. Guilderson, *Science* **292**, 1367 (2001).
25. J. Lean, D. Rind, *J. Atmos. Solar-Terr. Phys.* **61**, 25 (1999).
26. M. Stuiver, *J. Geophys. Res.* **66**, 273 (1961).
27. P. A. Mayewski *et al*., *J. Geophys. Res.* **102**, 26345 (1997).
28. W. S. Broecker, S. Sutherland, T.-H. Peng, *Science* **286**, 1132 (1999).
29. M. Cane, A. Clement, in *Mechanisms of Global Climate Change at Millennial Time Scales*, P. Clark, R. Webb, L. D. Keigwin, Eds. (Geophysical Monograph Series 112, American Geophysical Union, Washington, DC, 1999), pp. 373–383.
30. D. G. Martinson *et al.*, *Quat. Res.* **27**, 1, 1987.
31. D. Shindell *et al.*, *Science* **294**, 2149 (2001).
32. G. Bianchi, I. McCave, *Nature* **397**, 515 (1999).
33. For a cooling of 0.5° to 1°C accompanying the increases in drift ice (*1*), $\delta^{18}O$ would increase between 0.1 and 0.2‰ (*49*). Because the mean decrease in planktic $\delta^{18}O$ in MC52-VM29-191 (Fig. 2) is about 0.3‰, a 0.4 to 0.5‰ decrease in $\delta^{18}O$ due to salinity is required during each increase in drift ice. On the basis of the $\delta^{18}O$ of seawater from near the coring site in (*50*), 1‰ $\delta^{18}O$ of seawater = about 1.2 salinity units. Hence, a salinity decrease of about 0.5 to 0.6 salinity units is required to account for the observed decrease in planktic $\delta^{18}O$ at MC52-VM29-191.
34. R. R. Dickson, J. Lazier, J. Meincke, P. Rhines, J. Swift, *Prog. Oceanogr.* **38**, 241 (1996).

35. M. Holland, C. Bitz, M. Eby, A. Weaver, *J. Climate* **14**, 656 (2001).
36. B. Rudels, *Philos. Trans. R. Soc. London A* **352**, 287 (1995).
37. Y. Kushnir, *J. Climate* **7**, 141 (1994).
38. J. Lean, J. Beer, R. Bradley, *Geophys. Res. Lett.* **22**, 3195 (1995).
39. D. Rind, *J. Geophys. Res.* **103**, 5493 (1998).
40. H. Oeschger, U. Siegenthaler, U. Schotterer, A. Gugleman, *Tellus*, **27**, 168 (1975).
41. U. Siegenthaler, *J. Geophys. Res.* **88**, 3599 (1983).
42. O. Marchal, T. F. Stocker, R. Muscheler, *Earth Planet. Sci. Lett.* **185**, 383 (2001).
43. M. Stuiver, T. F. Braziunas, *Nature* **338**, 405 (1989).
44. R. B. Alley *et al.*, *Geology* **25**, 483 (1997).
45. J. Beer *et al.*, *Nature* **331**, 675 (1988).
46. M. Stuiver, P. Quay, *Science*, **207**, 11 (1980).
47. R. Muscheler, J. Beer, G. Wagner, R. C. Finkel, *Nature* **408**, 567 (2000).
48. G. M. Raisbeck *et al.*, *Mineral. Mag.* **62A**, 1228 (1998).
49. S. R. Epstein, R. Buchsbaum, H. A. Lowenstam, H. C. Urey, *Geol. Soc. Am. Bull.* **64**, 1315 (1953).
50. G. A. Schmidt, G. R. Bigg, E. J. Rohling. 1999. "Global Seawater Oxygen-18 Database" (www.giss.nasa.gov/data/o18data/).
51. U. Pflaumann *et al.*, *Paleoceanography*, in preparation.
52. S. Levitus, R. Gelfeld, *NODC Inventory of Physical Oceanographic Profiles. Key to Oceanographic Records Documentation No. 18* (National Oceanographic Data Center, Washington, DC, 1992).
53. R. Kwok, D. Rothrock, *J. Geophys. Res.* **104**, 5177 (1999).
54. S. J. Johnsen, D. Dahl-Jensen, W. Dansgaard, N. Gundestrup, *Tellus* **47B**, 624 (1995).
55. K. M. Cuffey, G. D. Clow, *J. Geophys. Res.* **102**, 26383 (1997).
56. J. Beer *et al.*, *Nature* **331**, 675 (1988)
57. J. McManus, D. Oppo, L. Keigwin, J. Cullen, G. Bond, *Quat. Res.*, in press.
58. J. McManus *et al.*, *Nature* **371**, 326 (1994).
59. G. Kukla, J. F. McManus, D.-D. Rousseau, I. Chuine, *Quat. Sci. Rev.* **16**, 605 (1997).
60. M. R. Chapman, N. J. Shackleton, *Geology* **27**, 795 (1999).
61. H. Lamb, *Climate, History and the Modern World* (Routledge, London, New York, ed. 2, 1995).
62. D. Dahl-Jensen *et al.*, *Science* **282**, 268 (1998).
63. H. Fischer *et al.*, *Geophys. Res. Lett.* **25**, 1749 (1998).
64. J. Hurrell, Y. Kushnir, M. Visbeck, *Science* **291**, 603 (2001).
65. M. Visbeck, H. Cullen, G. Krahmann, N. Naik, *Geophys. Res. Lett.* **25**, 4521 (1998).
66. G. Krahmann, M. Visbeck, G. Reverdin, *J. Phys. Oceanogr.* **31**, 1287 (2001).
67. L. Labeyrie *et al.*, in *Mechanisms of Global Climate Change at Millennial Time Scales*, P. Clark, R. Webb, L. D. Keigwin, Eds. (Geophysical Monograph Series 112, American Geophysical Union, Washington, DC, 1999), pp. 77–98.
68. C. Walebroeck *et al.*, *Paleoceanography* **13**, 272 (1998).
69. J.-C. Duplessy, L. Labeyrie, A. Juillet-Leclerc, J. Duprat, in *The Last Deglaciation: Absolute and Radiocarbon Chronologies*, E. Bard, W. S. Broecker, Eds. (NATO ASI Series I: Global Environmental Change, Springer-Verlag, Berlin, 1992), vol. 2, pp. 201–217.
70. Updated from M. Weinelt, M. Sarnthein, E. Jansen, H. Erlenkeuser, H. Schulz, in *The Younger Dryas*, S. Troelstra, J. van Hinte, G. M. Ganssen, Eds. (North-Holland, Amsterdam, 1995), pp. 109–115 [M. Weinelt, personal communication; sea-surface temperatures in this publication were estimated with the GLAMP 2000 method (*51*)].
71. R. Isarin, S. Bohncke, *Quat. Res.* **51**, 158 (1999).
72. L. Keigwin, G. A. Jones, S. Lehman, *J. Geophys. Res.* **96**, 16811 (1991).
73. L. Keigwin, R. Pickart, *Science* **286**, 520 (1999).

74. We thank J. Lynch-Stieglitz, M. Cane, R. Anderson, G. Kukla, J. Lean, and D. Shindell for comments on the manuscript. This work was supported in part by grants from the National Science Foundation and from the National Oceanic and Atmospheric Administration. Support for the core curation facilities of the Lamont-Doherty Earth Observatory (LDEO) Deep-Sea Sample Repository is provided by the National Science Foundation (grant OCE00-02380) and the Office of Naval Research (grant N00014-96-I-0186). This is LDEO contribution 6272.

23 August 2001; accepted 5 November 2001
Published online 15 November 2001;
10.1126/science.1065680
Include this information when citing this paper.

REPORTS

Oscillating Rows of Vortices in Superconductors

T. Matsuda,[1] O. Kamimura,[1] H. Kasai,[1] K. Harada,[1] T. Yoshida,[1] T. Akashi,[2] A. Tonomura,[1]* Y. Nakayama,[3] J. Shimoyama,[3] K. Kishio,[3] T. Hanaguri,[4] K. Kitazawa[4]

Superconductors can be used as dissipation-free electrical conductors as long as vortices are pinned. Vortices in high-temperature superconductors, however, behave anomalously, reflecting the anisotropic layered structure, and can move readily, thus preventing their practical use. Specifically, in a magnetic field tilted toward the layer plane, a special vortex arrangement (chain-lattice state) is formed. Real-time observation of vortices using high-resolution Lorentz microscopy revealed that the images of chain vortices begin to disappear at a much lower temperature, T_d, than the superconducting transition temperature, T_c. We attribute this image disappearance to the longitudinal oscillation of vortices along the chains.

When a magnetic field is applied to a type II superconductor, tiny magnetic vortices, typically arranged in a triangular lattice, form inside it (*1*) and play a crucial role in the practical use of superconductors as electrical conductors. Unless they are pinned, the vortices begin to flow when driven by an applied current, eventually suppressing superconductivity. In high-temperature superconductors, however, the vortex behaviors are more complicated because of their anisotropic layered structure (*2*). For example, at high temperature T and magnetic field H, a single vortex line can split itself into vortex pancakes in each layer that can be displaced and move independently in a liquid-like state (*2–4*). In this regime, no pinning occurs and the critical current vanishes. The information about the microscopic behaviors of the vortices is therefore indispensable for developing high–critical current materials.

The effect of the anisotropic layered structures also appears in the static arrangement of vortices. When the field direction is tilted away from the c axis, a triangular vortex-lattice state is transformed into an unconventional arrangement of vortices consisting of alternating domains of linear chains and triangular lattices (*5*). This phenomenon has recently attracted much attention but has not yet been fully understood, despite both theoretical (*6, 7*) and experimental (*5, 8*) investigations.

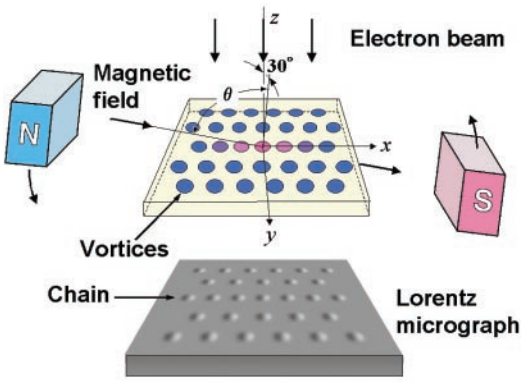

Fig. 1. Schematic of the experimental setup. A parallel electron beam was incident along the z axis onto a cleaved Bi-2212 thin film at $T = 10$ to 80 K. The film was tilted by 30° around the x axis, and a magnetic field H of 1 to 10 mT was applied to the film. When the electron image was defocused, vortices could be seen as spots of black and white contrasting regions. When the incident angle of the magnetic field direction to the film (θ) was greater than 70°, the vortex arrangement was not a conventional triangular lattice but consisted of alternating domains of linear chains and triangular lattices.

[1]Advanced Research Laboratory, Hitachi Ltd., Hatoyama, Saitama 350-0395, Japan. [2]Hitachi Instruments Service Co. Ltd., 4-28-8 Yotsuya, Shinjuku-ku, Tokyo 160-0004, Japan. [3]Department of Applied Chemistry, University of Tokyo, Tokyo 113-8656, Japan. [4]Department of Advanced Materials Science, School of Frontier Sciences, University of Tokyo, Tokyo 113-0033, Japan.

*To whom correspondence should be addressed. E-mail: tonomura@harl.hitachi.co.jp